

The Silicon Sensors for the High Granularity Calorimeter of CMS

Peter Paulitsch*, on behalf of the CMS Collaboration

Austrian Academy of Sciences, Institute of High Energy Physics (HEPHY), Nikolsdorfer Gasse 18, 1050 Wien, Austria

Abstract

The installation of the High-Luminosity Large Hadron Collider (HL-LHC) presents unprecedented challenges to experiments like the Compact Muon Solenoid (CMS) in terms of event rate, integrated luminosity and therefore radiation exposures. To cope with this new environment, new detectors will be installed during the CMS Phase 2 Upgrade, including the replacement of the calorimeter endcaps with a sampling calorimeter called "High Granularity Calorimeter" (HGCAL), which contains silicon sensors and scintillators as active elements. The silicon sensors will be produced in an 8" wafer process, which is new for high-energy physics. Due to its pioneering role, it demands extensive quality verification. The silicon sensors contain hexagonally shaped n-in-p DC-coupled diodes, which allow for maximization of the usable wafer area. A first batch of prototype sensors underwent electrical and irradiation tests at the institutes of the CMS Collaboration. Testing revealed major problems with the mechanical stability of the thin backside protective layer, that were not seen in earlier 6" prototypes those were produced by a different backside processing method. Following these results, CMS introduced the concept of "frontside biasing", allowing testing of the sensors without exposing its backside, verified the applicability, and adapted the prototype design to apply this method in series production.

Keywords: Compact Muon Solenoid, Large Hadron Collider, High-Luminosity, High Granularity Calorimeter, large area, silicon pad sensors

1. Introduction

During the Phase-2 Upgrade (2025 to 2027), the Large Hadron Collider (LHC) will be upgraded to the High-Luminosity LHC (HL-LHC). The HL-LHC will have a factor 5–7 higher instantaneous luminosity compared to the end of LHC operation, resulting in a proportionally higher pileup and a factor 10 increase in integrated luminosity (3000 fb^{-1}) over 10 years of operation. As a result, unprecedented levels of radiation and particle shower densities will affect experiments such as the Compact Muon Solenoid (CMS) [1]. To address these challenges, the CMS Collaboration will upgrade its subdetectors including a replacement for the existing endcap calorimeters with the new High Granularity Calorimeter (HGCAL), as shown in Figures 1 and 2). The calorimeter will utilize about $30,000^1$ sensor modules covering more than 620 m^2 , allowing for efficient mitigation of pileup and particle-flow calorimetry.

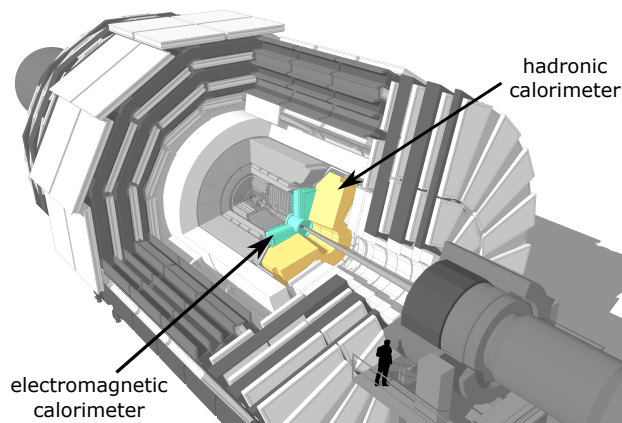


Figure 1: Location of the HGCAL at the CMS endcaps [2].

The HGCAL will be a sandwich calorimeter and will include an electromagnetic part (Calorimeter Endcap - Electromagnetic, CE-E) and a hadronic part (Calorimeter Endcap - Hadronic, CE-H). While the active sensing elements of the electromagnetic part will entirely be made of silicon sensors, the hadronic elements will be

*Corresponding author

Email address: peter.paulitsch@cern.ch (Peter Paulitsch)

¹preliminary, may be changed for optimizing calorimeter coverage

partially silicon sensors and scintillators coupled to silicon photomultipliers. This article focuses on the silicon parts of the CE-E and CE-H sections, as shown in Figure 2.

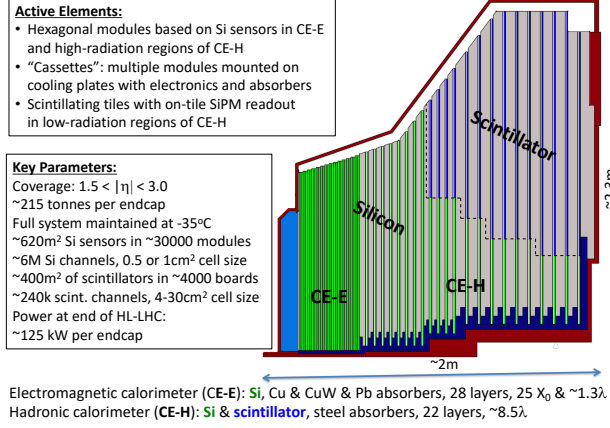


Figure 2: Schematic cross section of an endcap sector [3].

2. Silicon sensors for the HGCAL

The silicon sensors of the HGCAL will be produced in an 8" process [4], in contrast to earlier applications in high-energy physics, which used 6" processes. The leap towards the 8" process decisively reduces production costs and sensor testing efforts. However, this process is new to large-area sensors for high-energy physics and therefore brings new challenges.

Three different sensor thicknesses will be deployed: 120 μm, 200 μm and 300 μm to cope with different levels of radiation (Table 1). The 120 μm sensors will be manufactured in an epitaxial process, whereas the thicker will be produced in a float-zone process. The shape of a full sensor is hexagonal because a hexagon is the largest seamlessly tileable, regular shape on a circular wafer. This maximizes the wafer-area usage, reduces the number of necessary sensor tiles, hence decreases costs.

Consequently, the active sensing elements also have a hexagonal shape, except for some irregular cells at the sensor edges and corners. The diodes are n-in-p and DC-coupled. For the 200 μm and 300 μm thick sensors, the so-called "Low-Density" (LD) design with 192 full-size channels is chosen. To keep the cell capacitances low, the 120 μm thick sensors have smaller cells and therefore 432 full-size channels, the "High-Density" (HD) design as shown in Figure 4. Inside some cells, additional smaller circular, so-called calibration diodes

are integrated with lower surface and hence lower capacitance. These maintain sensitivity to minimum ionizing particles (MIP) after an integrated luminosity of 3000 fb⁻¹ at the end of the detector's life cycle.

Table 1: Active thicknesses d_{act} , number of channels, maximum expected fluences Φ_{neq} (normalized to 1 MeV neutron equivalent), and maximum expected total ionizing dose (TID) at 3000 fb⁻¹ [4].

full-size			
d_{act} (μm)	channels	Φ_{neq} (cm ⁻²)	TID (Gy)
120	432 (HD)	7.0×10^{15}	1×10^6
200	192 (LD)	2.5×10^{15}	2×10^5
300	192 (LD)	5.0×10^{14}	3×10^4

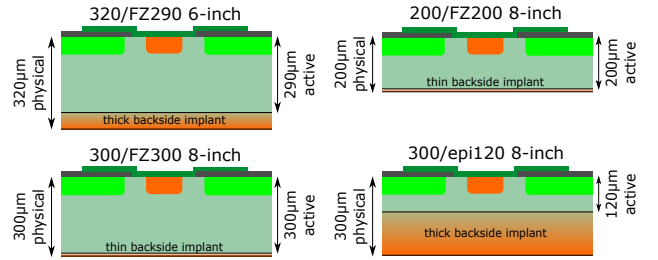


Figure 3: Sensor cross sections at different manufacturing processes. "epi" denotes an epitaxial process, "FZ" stands for "float-zone". For comparison, one 6" processed sensor cross section is shown. The thin backside implant of the FZ200 and FZ300 processes is about 1 μm thick.

To control the electric fields and to reduce the leakage current at the edge region, the sensor features two n^{++} doped guard rings; the inner one is connected to ground and the outer one is floating. A p^{++} doped edge ring is placed at the sensor edge, as shown in Figure 11.

3. Sensor testing

During the production phase, multiple CMS institutes will do quality control of 1–2 % of all produced sensors. Because of the large quantities of sensors produced, CMS needs fast and widely automatized test equipment. In semiconductor industry, probe-cards are a common standard for large-scale quality control because they provide a fast and reliable testing environment. Therefore the collaboration developed an open-source full wafer probe-card and switching system, called "ARRAY" [5].

Characterization of the sensors is primarily fulfilled by measuring current versus voltage (IV) and capacitance versus voltage (CV) curves. For all individual sensor

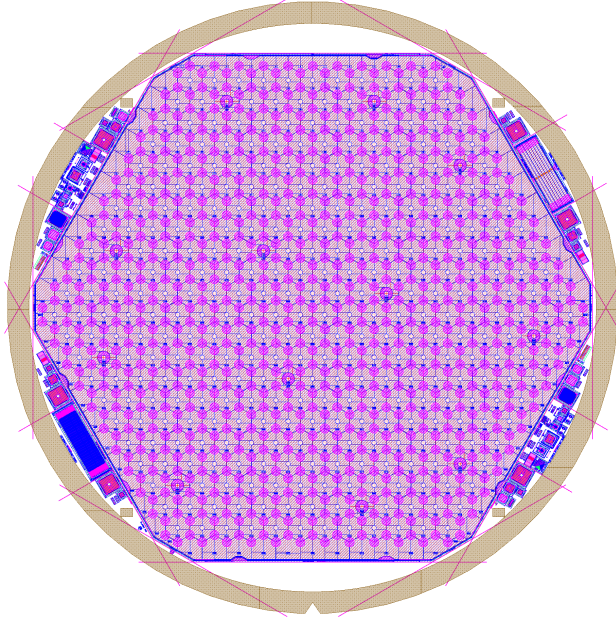


Figure 4: 432-channel (HD) full wafer design. The dashed squares at the wafer periphery mark the four test structure half moons [9].

cells on the same wafer, these measurements allow extracting parameters like the full depletion voltage (V_{fd}), full depletion capacitance (C_{fd}), or the breakdown voltage (V_{bd}).

4. Sensor backside sensitivity and scratch tests

Diode current characteristics on 8" HGCAL sensor prototypes showed a degradation in terms of an increasing number of cells with breakdowns between sensor handling procedures as shown in Figure 5. Repeated measurements without handling procedures in between remained stable. Because earlier 6" prototypes did not show this behavior, we suspected that the thin backside metalization of the 8" prototypes might cause early breakdowns and increased sensor currents. The previous 6" prototypes had a backside with a thick field stop implant ("deep-diffused"), seen on Figure 3.

To investigate these problems, scratch tests with a tungsten carbide needle were performed on test structures [6][7]. Using a needle manipulator, the needle tip (50 μm diameter) was kept hovering over the test structure diode, which was fixated to a precision scale (Kern 572-30, reproducibility 1 μg). The underlying table was raised until the needle touched the sensor surface and the scale displayed the desired weight. Subsequently, the table was moved to create a scratch. After each

scratch, the needle was removed and the diode IV characteristics were recorded, as shown in Figure 6. These tests showed that the diode's backside is highly sensitive to scratches, the breakdown voltage decreased with scratches made at higher needle weights and diode currents increased at deeper scratches.

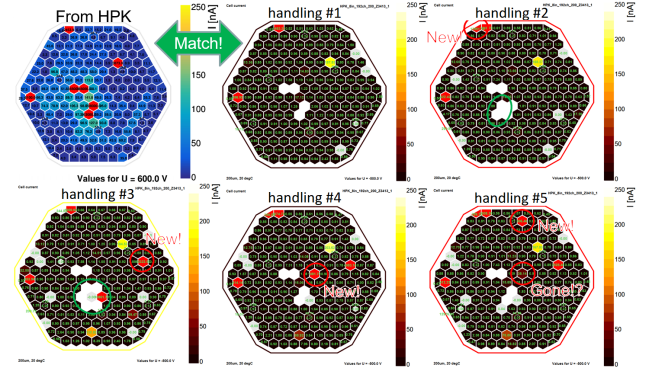


Figure 5: Sensor degradation after repeated handling steps for an unirradiated sensor, 192-channels, 200 μm active thickness. New breakdown cells (marked by circles) appeared after each handling step. Cells with values of "0.00" have bad contacts.

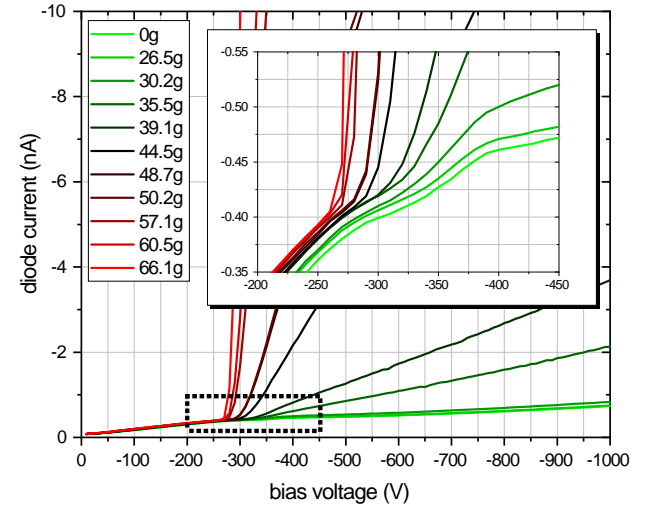


Figure 6: Test structure diode currents as a function of the bias voltage for increasing scratch depth, indicated by needle weight. The zoomed inlay shows a reduction of the breakdown voltage and increased currents with higher needle weight.

Depth measurements via laser interferometry (Wyko NT 3300 Profiling System) of these scratches showed that indeed the scratch depth increases with higher needle weight, and that all tried weights (10 g and more) penetrated the 1.1 μm backside aluminum layer. Vertical pressure tests with variable pressures of the

probe-card pins showed that the applied pressure of these pins did not alter the electrical characteristics of the diodes, even when measured during applied pressure, as shown in Figure 7.

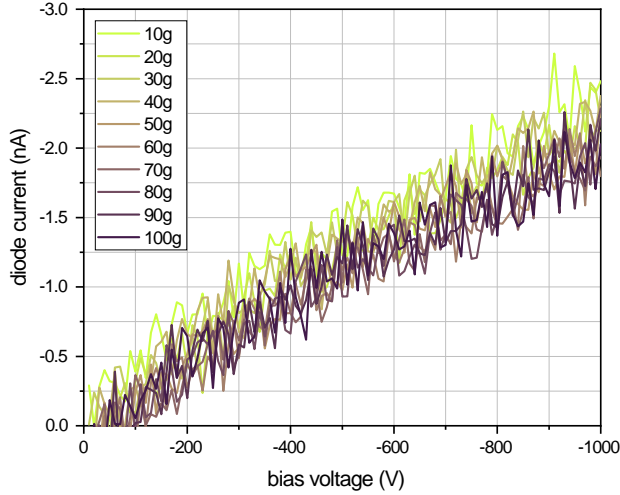


Figure 7: Test structure diode currents as a function of the bias voltage for increasing pin pressure, indicated by pin weight. No systematic behavior is seen at different pin pressures.

5. Frontside biasing and edge/guard ring extensions

Initially, it was planned to apply the bias voltage during testing via the sensor's backside aluminum metalization. Due to the aforementioned backside fragility, Hamamatsu discussed with the collaboration to glue a compound polyimide (Kapton™) foil on the backside during production to prevent scratches. This procedure would make it impossible to directly contact the backside. By exploiting the low-resistance path between edge ring, bulk and backside implant (all are p-doped, shown in Figure 8), it is possible to use the edge ring as a contact for sensor biasing instead. This method is referred as "frontside biasing" [8].

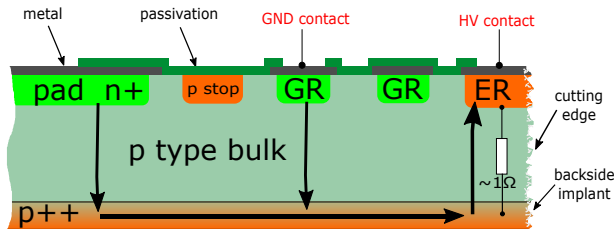


Figure 8: Sketch of cross section of the sensor edge using the frontside biasing concept. Current flow is visualized by the black arrows.

To verify this on the 8" prototypes, we tested frontside biasing on an unirradiated, 192-channel 200 μm thick sensor and compared frontside biasing cell currents to backside biasing cell currents. Figure 9 shows the relative spread as derived in Equation 1, between front side bias current I_{FSB} and back side bias current I_{BSB} for each cell.

$$R(\%) := \left| \frac{I_{\text{BSB}}}{a} - 1 \right| * 100\% \quad \text{and} \quad a = \frac{I_{\text{BSB}} + I_{\text{FSB}}}{2} \quad (1)$$

For most cells not in breakdown, the differences are below 2%. There were two exceptions with remarkable deviations up to 95%, which may have resulted in handling-induced defects (see Section 4) by changing to backside-biasing. Currents of cells in breakdown are not considered in this analysis.

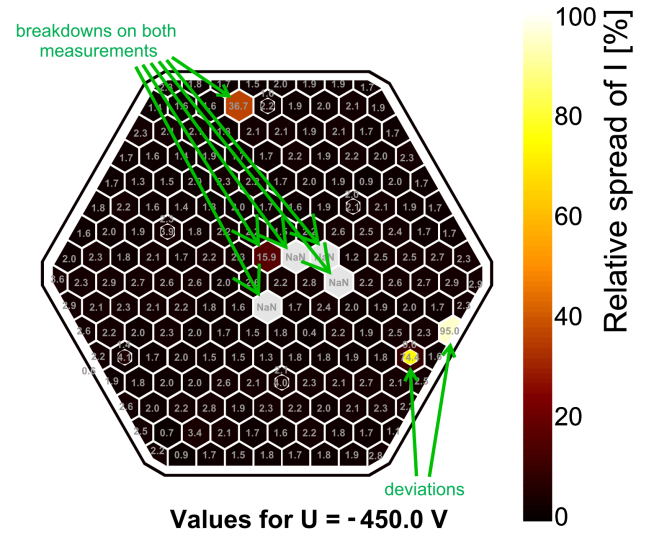


Figure 9: Cell current deviations between backside and frontside biasing of an unirradiated sensor, 200 μm thickness. Values are given in % (Equation 1) at -450 V.

The measured total currents deviated by less than 0.2% between frontside and backside biasing, as shown in Figure 10. Thus, we consider the frontside biasing concept as a viable option for unirradiated sensors.

In contrast to earlier sensor designs [7], inward extensions of the edge ring as shown in Figure 11 have now been included with contact pads (passivation openings over metalization). Since the HGCal will also utilize partial sensors, we applied one edge ring extension on each long sensor edge. These structures now give the possibility to contact the edge ring via probe-cards [5]. The contact area of the extensions is large enough to support two redundant pin contacts on each extension

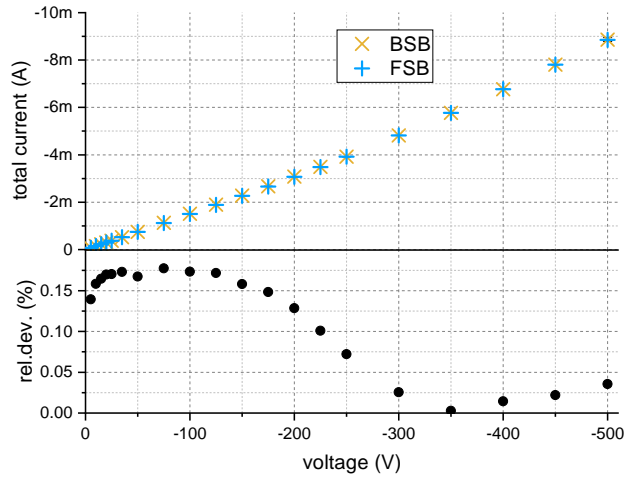


Figure 10: Total current as a function of the bias voltage, comparison between backside- and frontside biasing schemes for an unirradiated sensor, 200 μm active thickness. Relative deviations are given by Equation 1.

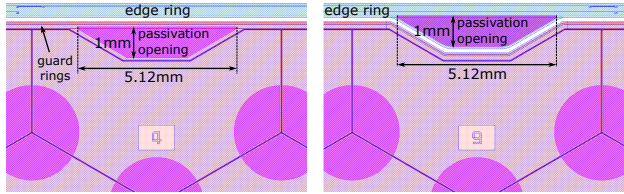


Figure 11: Extensions on the upper part of the sensor. Left: Trapezoidal guard ring extension. Right: Trapezoidal edge ring extension. The circular sectors are passivation openings to contact underlying structures.

to avoid sparking in case of loss contact during the testing.

For contacting the inner guard ring, we implemented a similar concept. The main purpose of these guard ring extensions, shown in Figure 11, is to ease placing wire-bonds between the guard ring and the "Hexaboard". The Hexaboard is a printed circuit board (PCB) for power supply and readout of the silicon sensor. A positive side-effect is the speedup of sensor testing because dedicated probe-card contacts using spring-loaded pins can be used instead of contacting the guard ring via separate needles. In previous designs, the guard ring was too narrow to be contacted via probe-card pins. However, 0.2036 % of active sensor area gets lost due to these extensions.

6. Prospects

To qualify the radiation hardness of the new 8" process, extensive irradiation tests have to be done. In-

dicators like full depletion voltage and bulk resistivity can be extracted from IV and CV measurements of the main sensors. Irradiation tests of test structures are planned. To investigate the p-stop structures, Metal-Oxide-Semiconductor Field-Effect Transistors (MOS-FETs) [9] can be used. MOS capacitor test structures allow measuring the oxide charges via flatband voltage, which gives information about the oxide quality.

It is projected to verify these results in parallel by Technology Computer-Aided Design (TCAD) simulations [7] to improve the understanding of the effects of the 8" process technology on radiation hardness.

Acknowledgements

This project has received funding from the call "Forschungspartnerschaften" of the Austrian Research Promotion Agency (FFG), Austria under the grant no. 868296.

References

- [1] The CMS Collaboration, The CMS experiment at the CERN LHC, Journal of Instrumentation 3 (08) (2008) S08004–S08004. doi:10.1088/1748-0221/3/08/s08004.
- [2] D. Barney, T. Sakuma, Sketchup images highlighting the sub-detectors (Sep 2017). URL <https://cds.cern.ch/record/2628519>
- [3] D. Barney, Overview slide of CE with main parameters (Oct 2019). URL <https://cms-docdb.cern.ch/cgi-bin/PublicDocDB/ShowDocument?docid=13251>
- [4] The CMS Collaboration, The Phase-2 Upgrade of the CMS Endcap Calorimeter, Tech. Rep. CERN-LHCC-2017-023. CMS-TDR-019 (2017). URL <https://cds.cern.ch/record/2293646>
- [5] E. Brondolin et al., ARRAY: An open source, modular and probe-card based system with integrated switching matrix for characterisation of large area silicon pad sensors, Nucl. Instrum. Meth. A940 (2019) 168–173. doi:10.1016/j.nima.2019.06.007.
- [6] V. Hinger et al., Process quality control for large-scale silicon sensor productions, Nucl. Instrum. Meth. A924 (2019) 38 – 43. doi:10.1016/j.nima.2018.07.082.
- [7] E. Pree, Development of large area silicon sensors for the high granularity calorimeter at CMS, Ph.D. thesis, Technische Universität Wien (2018). URL <http://katalog.ub.tuwien.ac.at/AC15192834>
- [8] M. Baselga et al., Front-side biasing of n-in-p silicon strip detectors, Journal of Instrumentation 13 (2018) P11007–P11007. doi:10.1088/1748-0221/13/11/P11007.
- [9] V. Hinger, Process quality control strategy for the Phase II upgrade of the CMS tracker and endcap calorimeters, Nucl. Instrum. Meth. A this volume (2020).